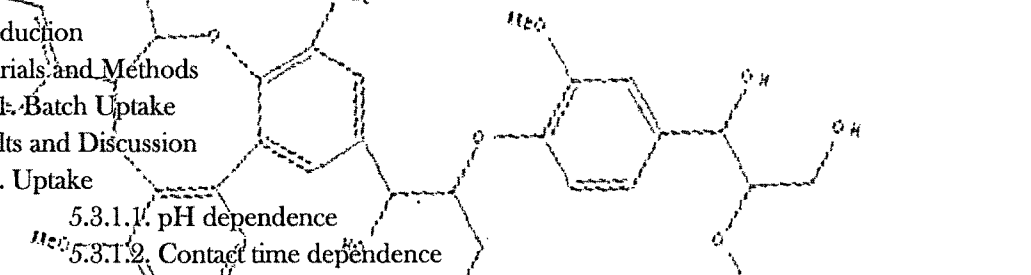


# Chapter 5

# Mechanistic and Spectroscopic study for adsorption of $U^{6+}$ onto the adsorbents prepared from Palm Shell Powder

### Outline:

- Outline:**

  - 5.1. Introduction
  - 5.2. Materials and Methods
    - 5.2.1. Batch Uptake
  - 5.3. Results and Discussion
    - 5.3.1. Uptake
      - 5.3.1.1. pH dependence
      - 5.3.1.2. Contact time dependence
      - 5.3.1.3. Dosage dependence
      - 5.3.1.4. Temperature dependence
    - 5.3.2. Adsorption Kinetics
    - 5.3.3. Adsorption Isotherms
    - 5.3.4. Thermodynamic Parameters
    - 5.3.5. FTIR spectroscopy
    - 5.3.6. X-ray Photoelectron Spectroscopy
    - 5.3.7. Column Studies
    - 5.3.8. Desorption Studies
  - 5.4. Mechanism
  - 5.5. Conclusions



## 5.1. Introduction

Biomaterials have also been investigated for their potential use in the remediation and/or recovery of uranium from aqueous solutions, high salt concentration solutions, acid mine drainage, and uranium process solutions (Table 1.1 of chapter 1) [1-8]. For uranium uptake, biosorbents of different origins viz., bacteria, fungi and plant biomass showing efficient metal uptake (>15% loading capacity) across the pH range 4–5.5 are common [9-11]. Yang and Volesky have investigated the interactions of uranyl cations with *Sargassum* seaweed, and they have modeled the interactions of proton exchange with uranyl cations [4]. In addition they have investigated the effect of pH on adsorption, which showed a pH-dependent trend and an increase in binding with an increase in pH. Jansson-Charrier et al. investigated the adsorption of uranium ions onto chitosan and found that it was effective in the treatment of leachates from mines [6]. Psareva et al. have investigated the sorption of uranium onto cork biomass [7]. Whereas, Liu et al. have studied the effects of cations and anions on the biosorption processes for uranium and found little or no effect from various cations and anions [8]. To the best of our knowledge there are no reports in the literature on biomass exhibiting good performance (>15% loading capacity) at low pH (~1). Hence use of these biosorbents for biosorption technology in treating such wastewaters becomes technically non-feasible. Furthermore, although studies on the biosorption of uranium have been performed, the investigation into the mechanism(s) of biosorption has not been studied to any great extent.

Spectroscopic techniques have been a valuable aid in determining functional groups that are responsible for metal binding. Parsons et al. have investigated the mechanism of uranium adsorption onto alfalfa biomass and have found that the primary functional group on alfalfa biomass responsible for the binding of uranyl cations from aqueous solution was the carboxyl functionality [12]. Several investigations have shown that U(IV) is formed during the adsorption of U(VI) [13-15]. However no investigation on speciation of uranium on biomass has been reported.

The objectives of the study were:

- 1) To explore the potential use of palm shell and palm shell based adsorbents for adsorption of uranium.
- 2) To study the influence of various parameters on adsorption.
- 3) To understand the adsorption mechanism through XPS and FT-IR spectroscopic techniques.

## 5.2. Material and Methods.

### 5.2.1. Batch Uptake.

A stock solution of  $U^{6+}$  was prepared by dissolving 2.11 g of uranyl nitrate (Sulab) in slightly acidified double distilled water and making upto 1L to give 1000 mg/L of uranyl solution. Working standards were prepared by diluting different volumes of the stock solution to obtain the desired concentration. Batch adsorption experiments were conducted as discussed in Chapter 3.

At the end of the predetermined time intervals, the suspensions were filtered and the filtrate was analysed to find the uptake of uranium by the adsorbents under study. The  $U^{6+}$  concentration in the filtrate was analysed spectrophotometrically by UV spectrophotometer (Elico SL177) after using Arsenazo as complexing agent [16].

## 5.3. Results and Discussion.

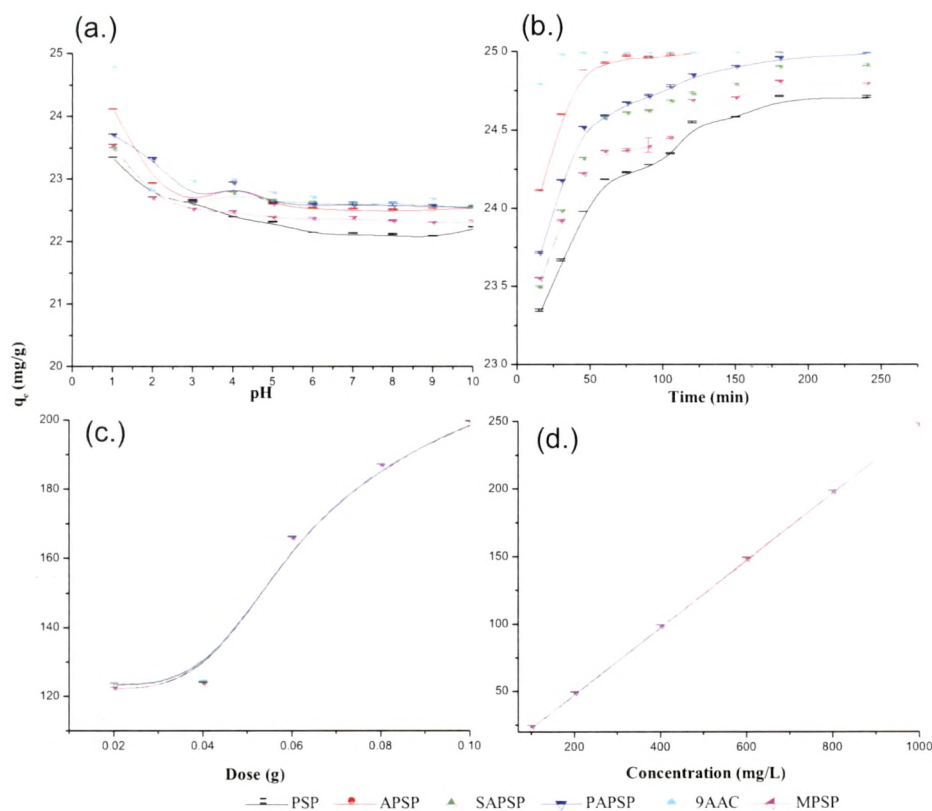
### 5.3.1. Uptake studies.

**5.3.1.1. pH dependence.** The effect of pH on the removal of uranyl ion (initial concentration 100ppm) was studied in the range 1 to 10.

Figure 5.1 shows that adsorption of uranyl ion was not much dependent on pH. Maximum adsorption occurs at pH 1 for all the adsorbents under study, followed by slight decrease till pH 5 and then remains constant for the remaining range of pH studied. However the percent adsorption varies to a maximum of around 6% in the entire pH range studied.

E. M. Saad et al. reported that the uptake of uranyl (II) ions is low at acidic  $pH \leq 5$ . The protonation of the available active sites (amino acids, hydroxyl and carboxyl groups) in the date pits most likely inhibit their binding towards the uranyl (II) ions as reported earlier by the same group [17-19] for the solid sorbent polyurethane foams thus lowering the  $UO_2^{2+}$  ions uptake from the aqueous media [20].

The maximum uranium adsorption at pH 1 suggests that electrostatic forces cannot explain the adsorption mechanism and that covalent bonding contributes significantly to the adsorption. However, the high extent of adsorption that occurs at higher pH values is likely due to a range of adsorption reactions because the aqueous speciation of uranium is so complex in this pH range.



Operating parameters: 30 °C, 180 rpm, pH 1, 100ppm of  $U^{6+}$ , 0.1g adsorbent, time 180 min, temperature 30 °C; Time variation: 30-180 min, pH variation: pH 1-10, Conc. variation: 100-1000 ppm, Dose variation: 0.02-0.10 g adsorbent

**Figure 5.1.** Effect of a) pH, b) time, c) dose, d) initial concentration of  $U^{6+}$

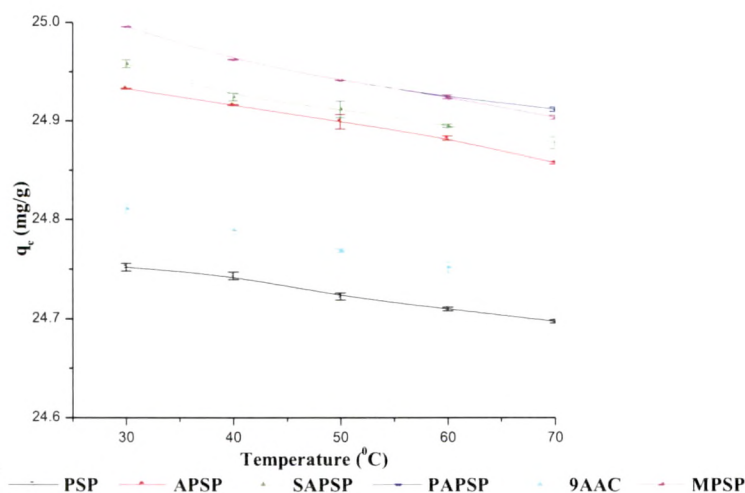
The predominate species in acidic solution up to pH =4.8 is  $UO_2^{2+}$  [21, 22]. The uranyl ion does not exist in the free state above pH 4, with uranyl hydroxide and uranyl-carbonate complexes dominating above pH 5, suggesting the adsorption of other uranium complexes to a significant extent. The relatively high extent of adsorption under these high pH conditions is likely caused by adsorption of the uranyl aqueous complexes themselves onto the adsorbent surface. The  $pK_a$  values of the protonation of the different functional groups in the adsorbents under study may account for the observed trend. The uptake at acidic pH could be attributed to the reducing action of aldehydes.

**5.3.1.2. Contact time dependence.** Contact time variation shows that equilibrium is achieved faster (30 & 80 min) when 9AAC & APSP was used as the adsorbent as compared to other

adsorbents under study (PSP, SAPSP, PAPSP and MPSP) where equilibrium was achieved in 180 min (Figure 5.1). The rate of adsorption is very fast initially with about 96% of total uranium being removed within few minutes followed by a decreased rate with the approach of equilibrium. The removal rate is high initially due to the presence of free binding sites which gradually become saturated with time resulting in decreased rate of adsorption as equilibrium approaches. This indicates that the adsorption is mainly through surface binding. Similar observations were made by Das et al [23].

**5.3.1.3. Amount of adsorbent variation.** The effect of dose of adsorbents under study on the removal of uranium is shown in Figure 5.1, which illustrates the adsorption of uranyl ion with change of the adsorbent dose from 200 to 1000 mg. As inferred from Figure 5.1, for a fixed metal initial concentration, increasing the adsorbent dose provided greater surface area and availability of more active sites [24], thus leading to the enhancement of metal ion uptake. Adsorption increased from 98 to >99% with increase in adsorbent dose.

**5.3.1.4. Temperature variation.** Temperature studies showed (Figure 5.2) almost the same trend for all the adsorbents under study. From the figure it can be seen that uptake decreases as temperature increases indicating that the mechanism of adsorption is exothermic in nature for all the adsorbents under study.

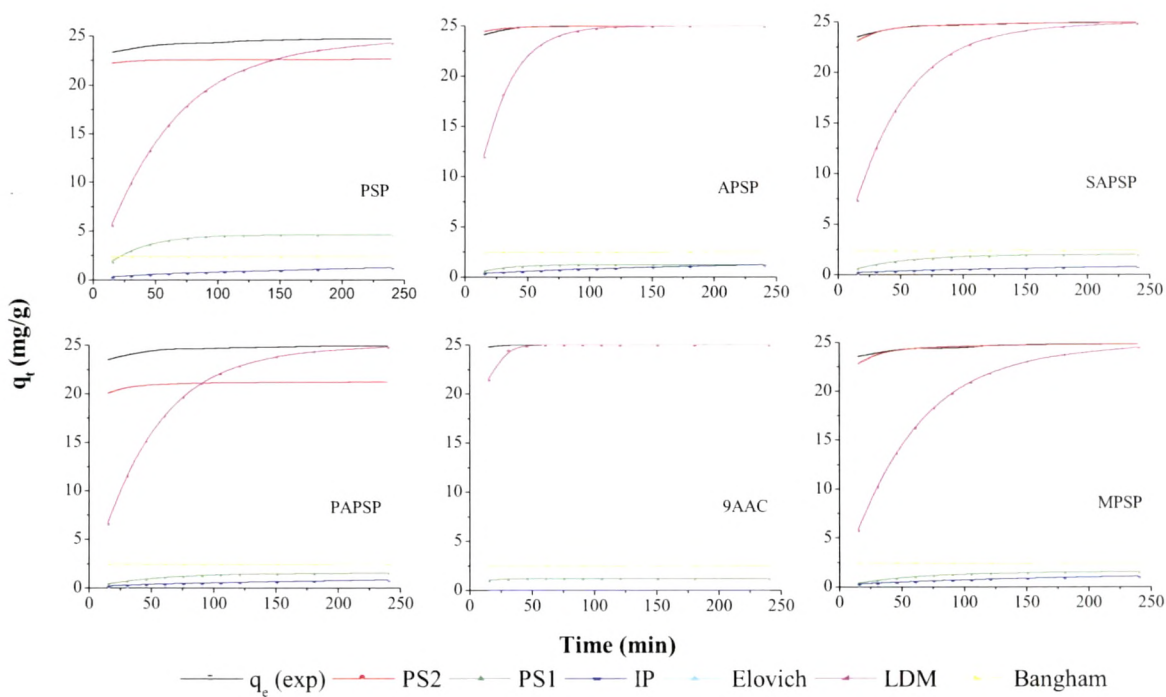


Operating parameters: 180 rpm, 0.1g adsorbent, time 240 min, optimum pH

**Figure 5.2.** Effect of temperature on uptake of uranyl ions by PSP, MPSP, APSP, SAPSP, PAPSP and 9AAC

5.3.2. Adsorption Kinetics.

Figure 5.3 shows the adsorption kinetics conducted at pH 1 for  $U^{6+}$  removal by PSP, APSP, SAPSP, PAPSP, 9AAC and MPSP. Adsorption of  $U^{6+}$  ions onto the adsorbents under study was carried out for 240 min. to ensure attainment of equilibrium. The kinetic models of Pseudo First order, Pseudo Second order, Intraparticle diffusion, Bangham, Elovich and Liquid film diffusion models were studied and the kinetic constants for the adsorption of mercury by all the adsorbents under study are presented in Table 5.1.



Operating parameters: 15-240 min, pH 1, 100 ppm of  $U^{6+}$ , 0.1 g adsorbent, 30  $^{\circ}$ C, 180 rpm.

**Figure 5.3.** Kinetic studies

**Table 5.1.** Kinetics parameters for uranium adsorption

<b>pH1</b>						
	<b>PSP</b>	<b>APSP</b>	<b>SAPSP</b>	<b>PAPSP</b>	<b>9AAC</b>	<b>MPSP</b>
<b>q<sub>e</sub> (exp)</b>	24.714	25.000	24.920	24.996	25.000	24.802
<b>Pseudo 2<sup>nd</sup> order</b>						
<b>q<sub>e</sub> (mg.g<sup>-1</sup>)</b>	22.629	25.056	25.044	21.286	62.112	24.944
<b>K<sub>2</sub> (g.mgmin<sup>-1</sup>)</b>	0.154	0.104	0.031	0.047	0.094	0.028
<b>r<sup>2</sup></b>	0.999	1.000	1.000	1.000	0.999	0.999
<b>SD</b>	0.017	0.005	0.008	0.007	6.24E-04	0.016
<b>Lagergren</b>						
<b>q<sub>e</sub> (mg.g<sup>-1</sup>)</b>	4.604	1.223	1.971	1.546	1.197	1.545
<b>K<sub>1</sub> (min<sup>-1</sup>)</b>	-0.035	-0.043	-0.023	-0.021	-0.129	-0.018
<b>r<sup>2</sup></b>	0.795	0.970	0.942	0.989	0.986	0.954
<b>SD</b>	0.082	0.067	0.101	0.075	0.098	0.111
<b>Intra Particle Diffusion</b>						
<b>K<sub>ip</sub>(mg/g/min)</b>	0.079	0.008	0.049	0.054	0.000	0.070
<b>r<sup>2</sup></b>	0.951	0.806	0.976	0.967	0.000	0.921
<b>SD</b>	0.072	0.016	0.030	0.039	0.000	0.082
<b>Elovich</b>						
<b>β (g.mg<sup>-1</sup>)</b>	1.907	3.478	1.969	2.204	1.865	2.158
<b>α (mg.g<sup>-1</sup>min<sup>-1</sup>)</b>	3.788E+41	3.66E+81	4.32E+43	3.83E+49	7.70E+45	8.89E+47
<b>r<sup>2</sup></b>	0.989	0.859	0.964	0.971	0.711	0.981
<b>SD</b>	0.065	0.107	0.119	0.096	0.046	0.079
<b>Liquid film diffusion model</b>						
<b>K<sub>FD</sub> (min<sup>-1</sup>)</b>	0.017	0.043	0.023	0.021	0.129	0.018
<b>r<sup>2</sup></b>	0.979	0.970	0.942	0.989	0.987	0.954
<b>SD</b>	0.095	0.085	0.097	0.103	0.106	0.163
<b>Bangham</b>						
<b>K<sub>BM</sub> (mL.g<sup>-1</sup>.L<sup>-1</sup>)</b>	-114.160	-113.179	-113.807	-113.635	-112.841	-113.918
<b>α</b>	1.02E-04	4.43E-05	9.15E-05	8.20E-05	7.28E-06	8.88E-05
<b>r<sup>2</sup></b>	0.881	0.616	0.798	0.811	0.455	0.863
<b>SD</b>	0.004	0.004	0.005	0.004	0.001	0.004

The pseudo second order kinetics provided the best fit for the kinetic data at all pH values. The q<sub>e</sub> values were very close to the experimental q<sub>e</sub> value and correlation coefficient

values were 0.99-1 at all the pH values for PSP, APSP, SAPSP, PAPSP, 9AAC and MPSP suggesting rate limiting step in adsorption of uranium could be chemisorption involving valence forces through the exchange of electrons between sorbent and sorbate [25, 26], complexation, coordination and/ or chelation.

In pseudo first order model the  $q_{e(\text{exp})}$  values were much higher than  $q_e$  fitted values showing large discrepancies demonstrating that the reaction cannot be classified as pseudo first order although this plot has reasonably good correlation coefficient from the fitting process. This underestimate of the amount of binding sites is probably due to the fact that  $q_e$  was determined from the y-intercept (0, 1). This has been observed by several other workers [27-30]. This could be due to boundary layer controlling the beginning of the adsorption process [30].

The curves for Liquid Film Diffusion Model (Table 3.1 Chapter 3) did not pass through origin as required by the model for all the adsorbents under study but had very small intercepts (curves not shown) indicating that diffusion of uranium from the liquid phase to the adsorbent surface might be having some role in deciding the rate processes.

The Weber and Morris adsorption kinetic model was plotted using the equation given in Table 3.1 (Chapter 3). The plots obtained for PSP, APSP, SAPSP, PAPSP, 9AAC and MPSP do not pass through origin implying that intraparticle diffusion is not the only operative mechanism. The intraparticle diffusion rate is fastest in PSP and APSP, the order being  $\text{APSP} \sim \text{PSP} > \text{MPSP} > \text{PAPSP} > \text{SAPSP} > \text{9AAC}$  as evident from intraparticle diffusion rate constants. Finally, in order to further confirm the occurrence of intraparticle diffusion, Bangham equation (Table 3.1 of Chapter 3) was applied to the adsorption data. The double logarithmic plots obtained with very less correlation coefficients ( $>0.455$ ) indicated very less contribution of pore diffusion towards adsorption process. The lowest  $r^2$  value for 9AAC is in agreement with the results of intraparticle diffusion. The not so linear curves indicated the diffusion of adsorbate into pores of the sorbent is not the only rate controlling step.

Adsorption capacity of the adsorbents for uranium was highest at pH 1 hence kinetics was studied at pH1, which is consistent with results of others [31]. Initial rapid uptake implies the binding of adsorbate ions on the surface of adsorbents under study through proton exchange at pH 1. Later on slower adsorption might be due to intraparticle diffusion, and diffusion of uranium from the aqueous phase to the adsorbent due to weak acidic and basic groups such as carboxyl, hydroxyl, amino groups at  $\text{pH} > 1$ .



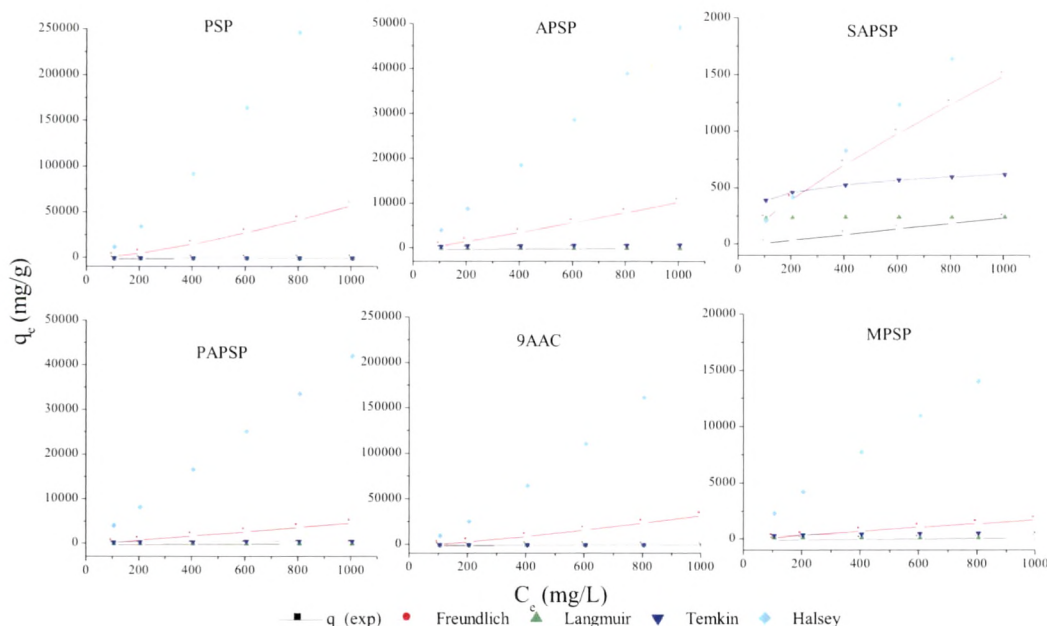
### 5.3.3. Adsorption Isotherms.

For modeling of mercury uptake Freundlich, Langmuir, Temkin, Dubinin-Radushkevich (DR), Flory-Huggins, Elovich and Halsey isotherm models were employed. Adsorption isotherms of the type  $q_e$  vs  $C_e$  were also used to verify the isotherm models. Model fits for all the isotherms along with experimental data for adsorption of  $U^{6+}$  on PSP, APSP, SAPSP, PAPSP, 9AAC and MPSP are presented in Figure 5.4. The values of model constants along with their correlation coefficients,  $r^2$  and SD values for all the systems studied are presented in Table 5.2.

Freundlich equation describes adsorption (possibly multilayer in nature) on a highly heterogeneous surface consisting of non identical and energetically non uniform sites. The value of  $n \approx 1$  for the Freundlich model indicates favorable adsorption. The Langmuir isotherm model is basically developed for gas-phase adsorption on homogeneous surfaces of glass and metals and predicts a single maximum binding capacity. The parameters  $K_L$  (equilibrium sorption constant) and  $q_{max}$  were calculated from the intercept and slope of the plot of  $C_e/q_e$  versus  $C_e$ . Based on the correlation coefficient  $r^2$  and standard deviations for Langmuir it varied from 0.958 to 0.999 with very less SD values. Langmuir monolayer adsorption capacity was found in good agreement with the experimental adsorption capacities.

**Table 5.2.** Isotherms parameters for different adsorbents

	PSP	APSP	SAPSP	PAPSP	9AAC	MPSP
$q_e$ (exp) (mg/g)	248.440	248.280	248.364	248.415	248.427	248.280
<b>Freundlich</b>						
$K_F(\text{mg.g}^{-1})(\text{dm}^3/\text{mg})^{1/n}$	3.739	4.618	5.989	5.207	4.226	5.474
n	0.714	0.893	1.248	1.008	0.770	1.188
$r^2$	0.989	0.977	0.991	0.988	0.961	0.998
SD	0.045	0.068	0.042	0.048	0.089	0.020
<b>Langmuir</b>						
$K_L (\text{dm}^3.\text{mg}^{-1})$	0.157	0.985	0.269	0.395	0.067	0.216
$q_m (\text{mg.g}^{-1})$	249.376	253.807	252.525	232.558	244.498	235.849
$\Delta G (\text{kJ.mol}^{-1})$	-4.810	-0.039	-3.407	-2.416	-7.017	-3.979
$r^2$	0.986	0.989	0.972	0.999	0.993	0.958
SD	1.90E-05	9.72E-04	0.001	2.48E-04	0.002	9.91E-04
<b>Temkin</b>						
$-\Delta H (\text{kJ.mol}^{-1})$	3.614	4.551	6.399	4.774	3.715	5.822
$K_T (\text{dm}^3.\text{mg}^{-1})$	0.639	0.867	0.570	0.869	0.748	0.725
$r^2$	0.995	0.995	0.994	0.989	0.994	0.978
SD	0.078	0.081	0.085	0.053	0.099	0.086
<b>DR</b>						
$q_m (\text{mg.g}^{-1})$	284.292	256.466	214.862	232.758	304.904	207.265
$E^0 (\text{KJ})$	14.041	17.330	12.883	12.918	1.498	15.377
$r^2$	0.991	0.985	0.964	0.973	0.998	0.953
SD	0.095	0.023	0.093	0.087	0.044	0.022
<b>Halsey</b>						
$K_H (\text{mg.g}^{-1})(\text{dm}^3/\text{mg})^{1/n}$	0.114	0.035	0.006	0.022	0.078	0.010
$n_H$	-0.714	-0.949	-1.248	-1.008	-0.770	-1.176
$r^2$	0.989	0.977	0.991	0.988	0.961	0.998
SD	0.094	0.056	0.098	0.098	0.094	0.046
<b>Flory-Huggins</b>						
$K_{FH} (\text{mg.g}^{-1})(\text{dm}^3/\text{mg})^{1/n}$	0.956	0.983	1.025	1.026	1.016	1.038
$N_{FH}$	-0.994	-0.998	-0.997	-0.997	-0.998	-0.995
$r^2$	1.000	1.000	1.000	1.000	1.000	1.000
SD	4.97E-04	4.06E-04	3.69E-04	7.78E-04	2.57E-04	6.08E-04
<b>Elovich</b>						
$q_m (\text{mg.g}^{-1})$	237.461	232.758	208.513	217.022	262.434	198.3434
$K_E (\text{dm}^3.\text{mg}^{-1})$	0.846	0.092	0.018	0.419	0.080	0.238
$r^2$	0.986	0.996	0.974	0.978	0.983	0.989
SD	7.39E-04	0.012	0.030	0.079	0.030	0.037



Operating parameters: 100-1000 ppm of  $U^{6+}$ , pH 1, 240 min, 0.1 g adsorbent, 30  $^{\circ}C$ , 180 rpm.

**Figure 5.4.** Adsorption Isotherms for  $U^{6+}$

The correlation coefficients of Temkin Model (0.978 to 0.995) indicate a satisfactory fit of the model to the experimental data. The variation of adsorption energy,  $\Delta Q = (3.614, 4.551, 6.399, 4.774, 3.715 \text{ and } 5.822)$  is positive for all the sorbents under study, which indicated the adsorption process to be exothermic.

The Dubinin–Radushkevich model is applied in the form of linear equation as given in Table 3.1 (Chapter 3). The adsorption energy values calculated for  $U^{6+}$  on PSP (14.041  $KJmol^{-1}$ ), APSP (17.330  $KJmol^{-1}$ ), SAPSP (12.883  $KJmol^{-1}$ ), PAPSP (12.918  $KJmol^{-1}$ ), 9AAC (1.498  $KJmol^{-1}$ ) and MPSP (15.377  $KJmol^{-1}$ ). The magnitude of  $E$  is useful for estimating the mechanism of the sorption reaction. In case of  $E < 8.0$  kJ/mol, physical forces may affect the sorption; for  $E$  in the range 8–16 kJ/mol, ion exchange is the working mechanism, while for  $E > 16$  kJ/mol sorption may be dominated by particle diffusion [32, 33]. It is thus evident from D-R model that for 9AAC physisorption is the predominant mechanism, while for APSP, SAPSP, PAPSP and MPSP ion-exchange is the predominant mechanism.

Multilayer adsorption is generally discussed by the Halsey equation and is found to fit well with the experimental data having  $r^2 (\geq 0.971)$  [25] indicating that the mechanism may be multilayer sorption for adsorbents under study while the low values of  $K_H$  suggest that multilayer sorption might be playing only a small role.

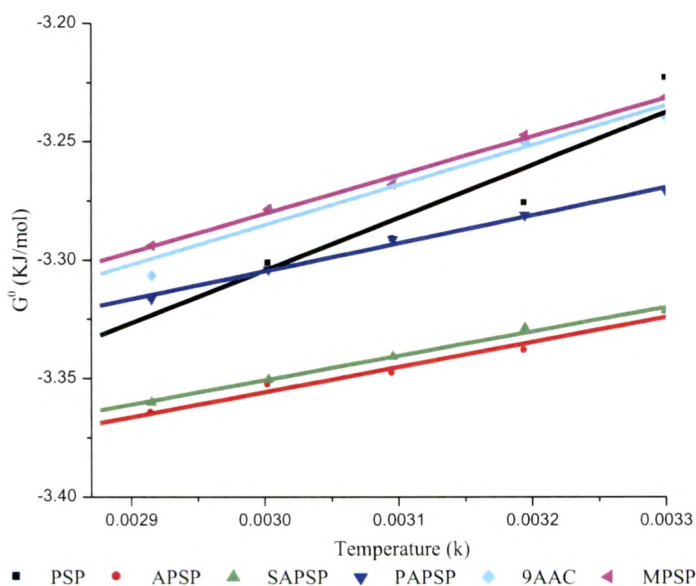
The Flory-Huggins model was used to assess the isotherm data. From the linear plots of  $\log(\theta/C_0)$  versus  $\log(1-\theta)$  (Figure not shown) for uranium adsorption on the adsorbents under study and the correlation coefficient values ( $r^2 = 1.00$ ), it is apparent that the model shows good fits for the adsorbent under study. However the negative values of  $n$  and low values of  $k_{FH}$  imply that the model cannot be used to describe the adsorption data.

#### 5.3.4. Thermodynamic Parameters.

The thermodynamic parameters of the sorption process could be determined from the experimental data obtained at various temperatures using the equations:

$$\Delta G^0 = \Delta H^0 - T\Delta S^0$$

The values of  $\Delta H^0$  and  $\Delta S^0$  can be calculated from the slope and intercept of the plots of  $\Delta G^0$  against  $T$  (Figure 5.5).



Operating parameters: 30-70 °C, 180 min, pH 1, 1000 ppm of  $U^{6+}$ , 0.1 g adsorbent, 180 rpm.

**Figure 5.5.** Thermodynamic studies

The negative value of  $\Delta H^0$  indicates that the adsorption of  $U^{6+}$  on PSP, APSP, SAPSP, PAPSP, 9AAC and MPSP is exothermic. Generally the absolute magnitude of the change in energy for physisorption is between (-20 and 0 KJ/mol); chemisorption has a range of (-400 and -80 KJ/mol). The negative value of  $\Delta G^0$  in table 5.3 indicates that sorption of uranyl ion by PSP, APSP, SAPSP, PAPSP, 9AAC and MPSP to be physisorption and is spontaneous and thermodynamically favorable [34].

**Table 5.3.** Thermodynamic Parameters for uranyl ions by PSP, APSP, SAPSP, PAPSP, 9AAC and MPSP

	$\Delta G$ (KJ/mol)	$\Delta S$ (KJ/molK)	$\Delta H$ (KJ/mol)	$r^2$	SD
PSP	-11.862	0.033	-1.854	0.945	0.001
APSP	-10.134	0.031	-0.881	0.986	0.003
SAPSP	-10.076	0.030	-0.856	0.997	0.002
PAPSP	-10.201	0.030	-0.981	0.996	0.002
9AAC	-10.941	0.032	-1.396	0.977	0.006
MPSP	-10.852	0.031	-1.355	0.997	0.002

Also the  $\Delta G^0$  values become less negative with increase in temperature suggesting that adsorption is favored at lower temperatures and hence is exothermic. The positive values of  $\Delta S^0$  suggest increased randomness during adsorption and a high affinity of the adsorbent towards the adsorbate.

### 5.3.5. FT-IR Spectroscopic Analysis.

FTIR spectra of uranium loaded PSP, APSP, SAPSP, PAPSP and MPSP are presented in Figure 5.6. The absorption bands of FTIR spectra listed in Table 5.4 reveal the changes in absorption bands of the surface functional groups of PSP, APSP, SAPSP, PAPSP, 9AAC and MPSP after uranium adsorption.

The band at 1720-1762  $cm^{-1}$  band is associated with C=O stretching mode of carbonyls in carboxylic acids and lactones while 1280-1000  $cm^{-1}$  band is associated with C-O stretching and O-H bending modes of groups such as phenols and carboxylic acids [35]. Also there is a shift in the frequencies of the absorption band of both C=O and C-O in carboxyl group (-COOH) due to metal binding.

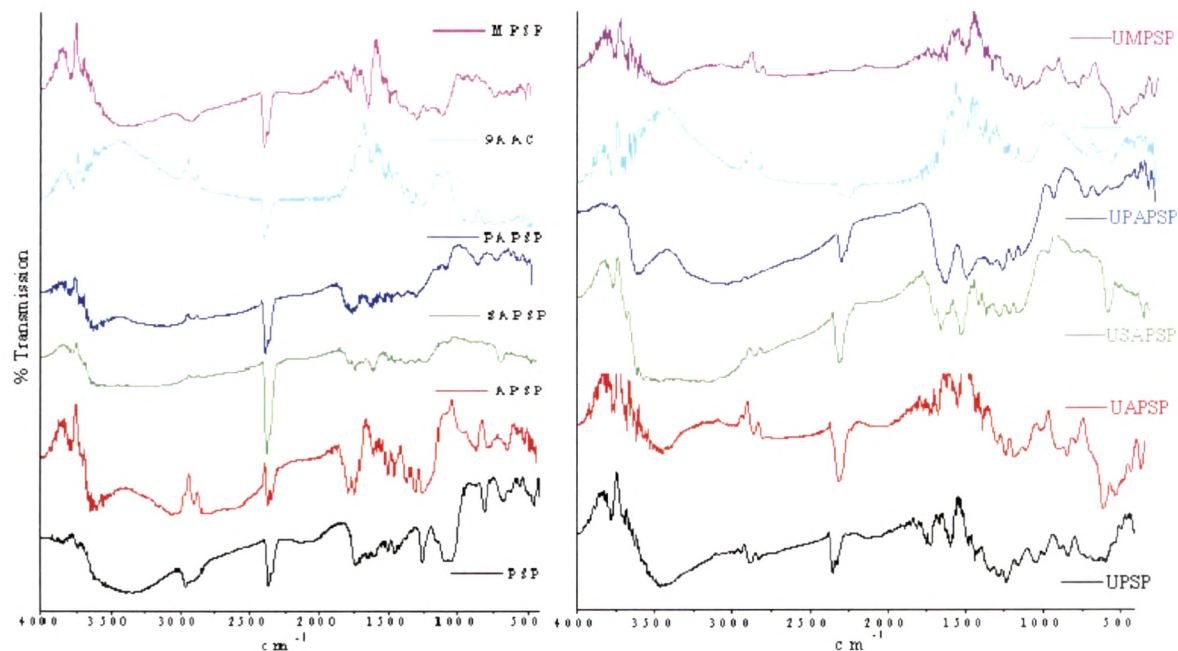


**Figure 5.6.** FTIR spectra of uranium loaded adsorbents

The C-O band shifts to higher frequencies 1217-1289  $\text{cm}^{-1}$  probably due to high electron density induced by the adsorption of U(VI) on the adjacent carbonyl groups [36, 37]. This showed that the carboxyl groups and metal ion were coordinated, which may have been caused by the oxygen atom of carboxyl groups coordinating with the metal ion and leading to the shifting of symmetrical stretching vibration of carboxyl groups ( $\nu\text{C=O}$ ). Similar observations were also made by Liu and Lin et al. [38, 39].

The band at 1720- 1732  $\text{cm}^{-1}$  which is the absorbing band of carboxyl groups almost disappeared after adsorption of uranium. This can be interpreted by the decarboxylation of carboxyl groups and the oxidation of quinone groups [41-42]. Thus carboxylic groups are involved in adsorption of uranium as seen by comparison of IR spectra of the adsorbents and the uranium loaded-adsorbents.

The interaction between uranium and carboxylic group of the adsorbent causes a diminution of the distance between C=O and C-O stretching peaks [43]. New peaks at wave numbers of 905-916  $\text{cm}^{-1}$  were observed in the uranium treated samples, these peaks can be assigned to the asymmetric stretching vibration of  $\text{UO}_2^{2+}$  [44, 45]. This peak was stronger in APSP, SAPSP, PSP than in MPSP, PAPSP and 9AAC suggesting higher uranium adsorption.



**Table 5.4.** Typical Absorption frequencies and Carbonyl stretching frequencies of Infra red spectra for free and metal loaded adsorbents

PSP-U	MPSP-U	APSP-U	SAPSP-U	PAPSP-U	9AAC-U	Assignment	
3451	3478	3465	3454	3613	-	-N-H, -O-H stretching	
2878, 2819	2979, 2875	2982, 2876	2893	3092, 2929	2990, 2876	-CH <sub>3</sub> , -CH <sub>2</sub> symmetric stretch	
2361	2345	2312	2335	2346	2335	Free CO <sub>2</sub>	
1718	1742 U <sup>4+</sup>	1752	1751	1688	-	-C=O stretch for acids or aldehyde	
1600	1586	1588	1589	1557	1591	-C=O stretch cellulose/ C=C Aromatic stretch (skeletal vibration)/ N-H bending of amide	
1487	1466	1482	1483	1415	1482	-CH <sub>2</sub> - stretch/ -C=C- Aromatic stretching	
1420	-	-	-	-	-	U <sup>3+</sup>	
1346	1331	1344	1351	1325	1347	-C-H stretch/ N-H bending	
1287	1274	1286	1289	1263	1217	-C-O bending of carboxylic acids/ phenolic O-H stretch/ N-H bending	
1163	1149	1168	-	1194	-	-O-H stretch (2 <sup>o</sup> Alcohol), -C-O-C- stretching	
1061 U <sup>6+</sup>	1051	1063 U <sup>6+</sup>	1041	1041	-	-C-H stretch, -C-O stretch (1 <sup>o</sup> Alcohol)	
888	889	-	-	-	-	Anomeric C-H bending of cellulose	
819	837 U <sup>6+</sup>	840	-	830 U <sup>6+</sup>	846	-C-H out of plane bending pentavalent uranium asymmetric stretch	
995 U <sup>6+</sup> , 850,571	947 U <sup>6+</sup> , 852,556	962 U <sup>6+</sup> , 844,570	948 U <sup>6+</sup> , 847, 573	950 U <sup>6+</sup> , 853, 569	950 U <sup>6+</sup> , 851,572	U-O bending vibrations $\nu_{as}$ axial strong band of U=O, Equatorial U-O stretching	
<b>Biosorbent</b>	$\nu_{C=O}$	$\nu_{C-O}$	$\Delta = \nu_{C=O} - \nu_{C-O}$	<b>Biosorbent</b>	$\nu_{C=O}$	$\nu_{C-O}$	$\Delta = \nu_{C=O} - \nu_{C-O}$
PSP	1732	1250	482	PSP-U	1718	1287	431 .
APSP	1720	1229	491	APSP-U	1752	1286	468
SAPSP	1723	1229	494	SAPSP-U	1751	1289	462
PAPSP	1723	1256	467	PAPSP-U	1688	1263	425
MPSP	1727	1238	489	MPSP-U	1742	1274	468

This indicates that part of uranium adsorption occurs by chemical adsorption (complexation) of uranyl species without reduction. The axial strong bands pertaining to the  $\nu_{as}(U=O)$  vibrational modes, were found at 995, 947, 962, 948, 950 and 950 cm<sup>-1</sup>, respectively. The two equatorial U-O stretching bands were at 571, 556, 570, 573, 569 and 572 cm<sup>-1</sup> respectively [46]. The uranyl asymmetric stretch for pentavalent uranyl complexes is observed in the IR spectrum at ~800 cm<sup>-1</sup> and is at significantly lower energy than the hexavalent uranium (~900 cm<sup>-1</sup>) [47].

### 5.3.6. X-ray Photoelectron Spectroscopic analysis.

To evaluate adsorption mechanism for adsorption of uranium onto PSP, APSP, SAPSP, PAPSP, 9AAC and MPSP was analysed by XPS. The XPS survey spectrum consisted of carbon, oxygen, nitrogen and uranium. Figure 5.7 shows the U 4f spectra of U(VI) adsorbed on PSP, APSP, PAPSP, SAPSP, 9AAC and MPSP at pH 1.0. The chemical shift in the U 4f7/2 peak position is directly related to the oxidation state of uranium. Its binding energy decreases as the oxidation state is decreased from VI to IV. However, uranium V and uranium VI oxidation states exist as  $\text{UO}_2^+$  and  $\text{UO}_2^{2+}$  ions [48]. As a consequence of this oxygen bonding, the chemical shift between V and VI states are reported to differ only marginally in the BE scale [49]. Furthermore, low intensity excitations result in shake-up satellites for both U 4f7/2 and U 4f5/2 states [49], as a consequence of the change in electrostatic potential during the photoelectron excitation process. The BE of the U 4f satellite peak is much more sensitive to the valence state than the BE of the main U 4f peak, so that they can be used as a probe to identify the oxidation state of uranium [50].

The BE's and the FWHM's of the peaks were obtained by a fit which includes four peaks on a Shirley background. The unusually large FWHM and the asymmetry towards low binding energies of these peaks suggest the presence of at least three different chemical environments inducing a different chemical shift. The results from XPS suggest that adsorption of uranyl ion from an aqueous solution results in a mixture of U(VI), U(V) and U(IV) oxidation states on the surface of all the adsorbents under study. The intense peaks at about 380 and 392 eV correspond to the spin-orbit (L-S) split U 4f7/2 and U 4f5/2 states, respectively. The 4f peak separation was found to be ~9 to 10 eV for each oxidation state of uranium. However, there also appears satellite peaks at a few eV slightly higher than the normal BE. Since the spin-orbit interaction separates these two levels by 10.85 eV, and hence the satellites of 4f7/2 which generally appear in this energy range are buried in the intense 4f5/2 peak or as a shoulder. These, satellite peaks carry the valence band information and are a good probe to identify chemical state and understand the chemical interaction [50]. This is applicable for both the U4f7/2 and U4f5/2 peaks. Since the spin-orbit interaction separates these two levels by 10.85 eV, and hence the satellites of 4f7/2 which generally appear in this energy range buried in the intense 4f5/2 peak or may appear as shoulder.



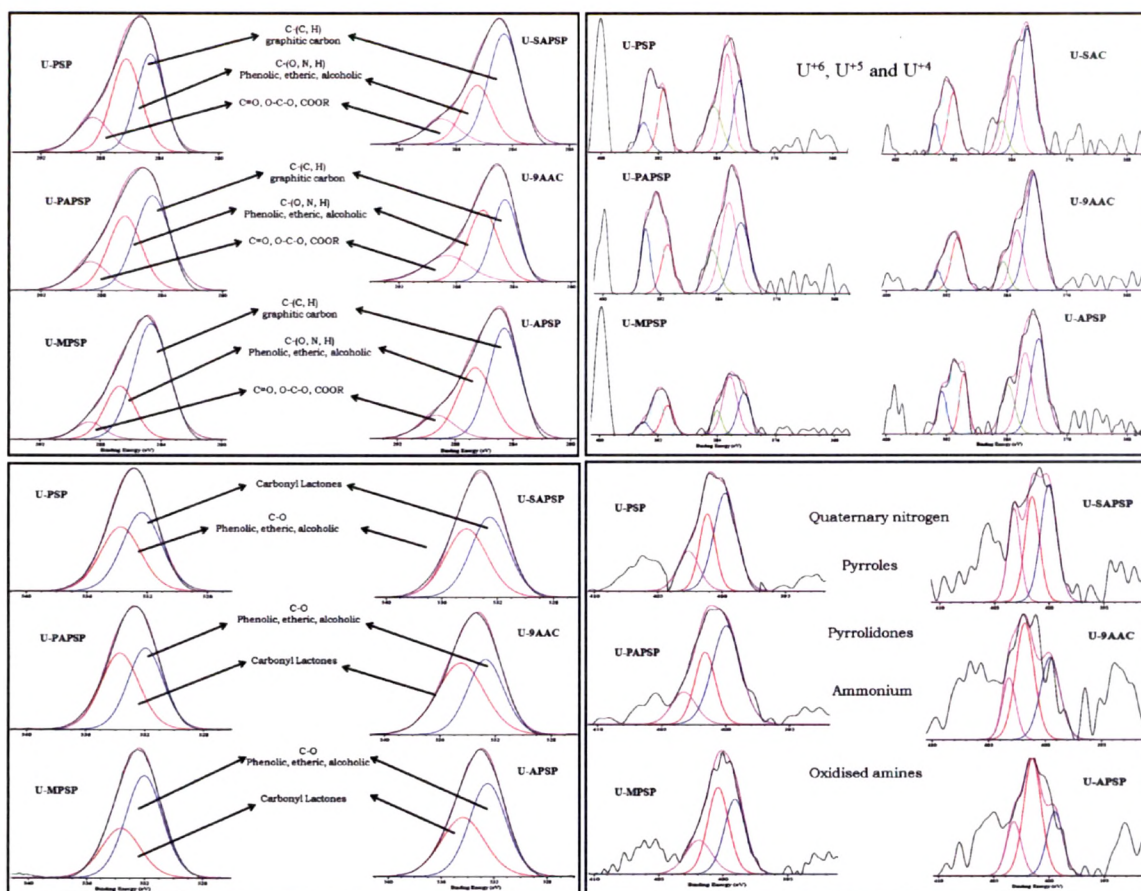


**Figure 5.7.** Deconvoluted XPS spectra of U

In the case of U (IV), the 5.8 and 16 eV satellites of 4f7/2 are clearly seen. Pireaux et al. [51] have reported satellites for U(IV) at 5.8, 8.2 and 16 eV higher binding energy than 4f photo peak position. The satellite peak observed at 397.0 eV, 397.6 eV which are approximately 7 eV from the U(4f5/2) peak, may be attributed to a shake-up transition from the oxygen-derived 2p band to the U(5f) Fermi level of UO<sub>2</sub> [50, 52]. The spectra contains two O1s peaks positioned at ~532 and ~534 eV, which can be assigned to terminal OH and sorbed H<sub>2</sub>O, respectively [53]. The peak position of U(V) was found to be 381.6 eV with FWHM 2.2 eV [49] and the satellite peaks appear at 7.9-8.1 eV from the main U4f7/2 and U4f5/2 peaks [50].

### 5.3.7. Column.

The column breakthrough curves for uranium adsorption by adsorbents under study are shown in Figure 5.8. The effluent concentration is seen to have the typical ‘S’ shape. A total of ~ 2.8 L of 1000 mg/L metal ion solution was passed through the column containing 5 g of

adsorbent under study. As seen from Figure 5.8 the breakthrough for uranium is seen to take place at 279.3, 147.2, 135.1, 129.1, 179.3 and 239 bed volumes for PSP, APSP, SAPSP, PAPSP, 9AAC and MPSP respectively.

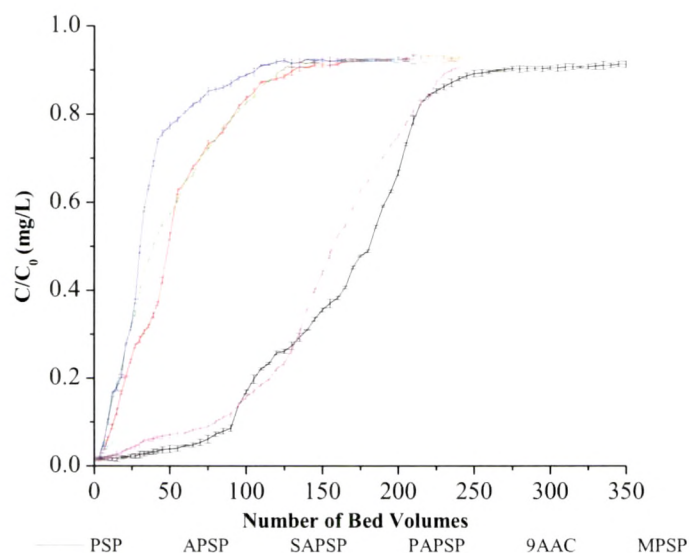


**Figure 5.8.** Column studies

**Table 5.5.** Column Isotherms parameters for different adsorbents

	PSP	APSP	SAPSP	PAPSP	9AAC	MPSP
<b>Thomas Model</b>						
$K_{TH}(\text{dm}^3/(\text{mg min}))$	0.00000443	0.00000435	0.00000389	0.00000424	0.00000453	0.00000503
$q_0 (\text{mg.g}^{-1})$	184.198	67.310	54.498	37.981	88.609	158.767
$r^2$	0.980	0.882	0.877	0.818	0.915	0.995
SD	0.074	0.085	0.086	0.093	0.766	0.091
<b>Yoon &amp; Nelson Model</b>						
$K_{YN} (\text{min}^{-1})$	4.43E-03	4.35E-03	0.00389	0.00424	0.00453	0.00503
$t_{0.5} (\text{exp}) (\text{min})$	950	335	292	189	451	789
$t_{0.5} (\text{cal}) (\text{min})$	920.993	336.551	272.494	191.038	443.046	794.035
$r^2$	0.980	0.882	0.877	0.818	0.915	0.996
SD	0.073	0.088	0.086	0.093	0.076	0.081
<b>Wolborska Model</b>						
$\beta (\text{min}^{-1})$	0.917	0.423	0.346	0.337	0.509	0.894
$N_0(\text{mg.dm}^{-3})$	348775.700	229873.900	231018.700	199769.200	241528.663	293228.900
$r^2$	0.936	0.724	0.697	0.646	0.774	0.973
SD	0.063	0.067	0.068	0.073	0.095	0.069

Thomas and Yoon–Nelson models were also applied to the column adsorption data at a flow rate of 1 mL/min at an initial metal ion concentration of 1 g/L and bed height 5 cm with all the adsorbents under study. From the linear plots of  $\ln[(C_o/C_t)-1]$  versus  $V_{eff}$  (Figure not shown) Thomas rate constant ( $k_{Th}$ ) and bed capacity ( $q_{Th}$ ) were calculated and are presented in Table 5.5.

The theoretical predictions based on the model parameters are compared in Figure 5.9 with the observed data. Similarly, from the plot of sampling time ( $t$ ) versus  $\ln[C_e/(C_o - C_e)]$ , the Yoon and Nelson constant  $K_{YN}$  and  $\tau$  (the time necessary to reach 50% of the retention) were calculated and are shown in Table 5.5.

The well fit of the experimental data on to the Thomas and Yoon-Nelson model indicate that external and internal diffusion will not be the limiting step. From the equations in Table 3.1 (Chapter 3) it is evident that the characteristic parameter associated with Thomas and Yoon and Nelson models vary but both the models predict essentially same uptake capacity and  $C/C_o$  values for a particular experimental set of data. Hence same  $r^2$  and SD values were obtained as also suggested by Baral et al. [54].

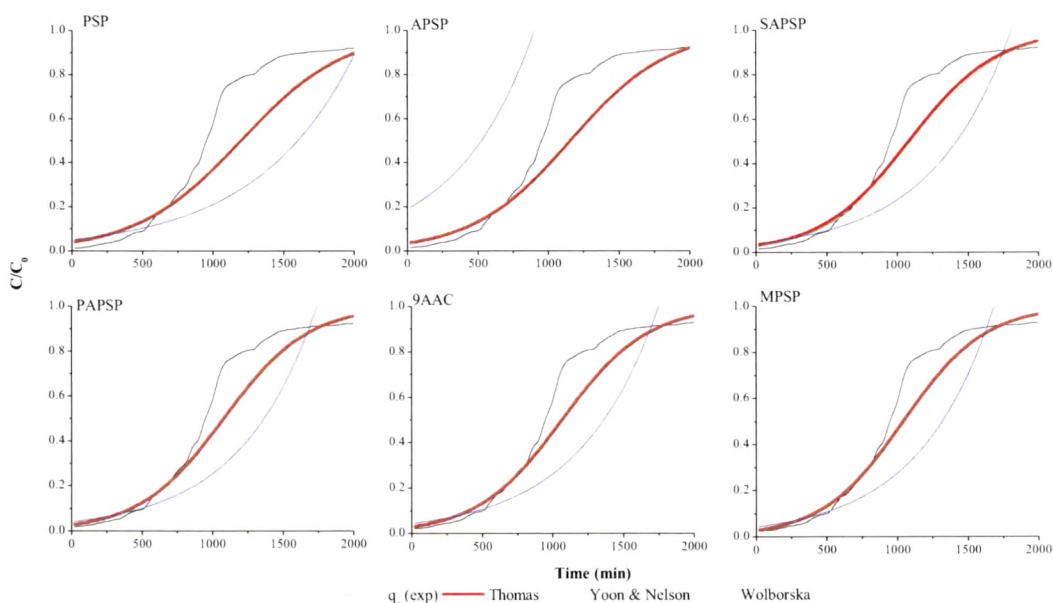
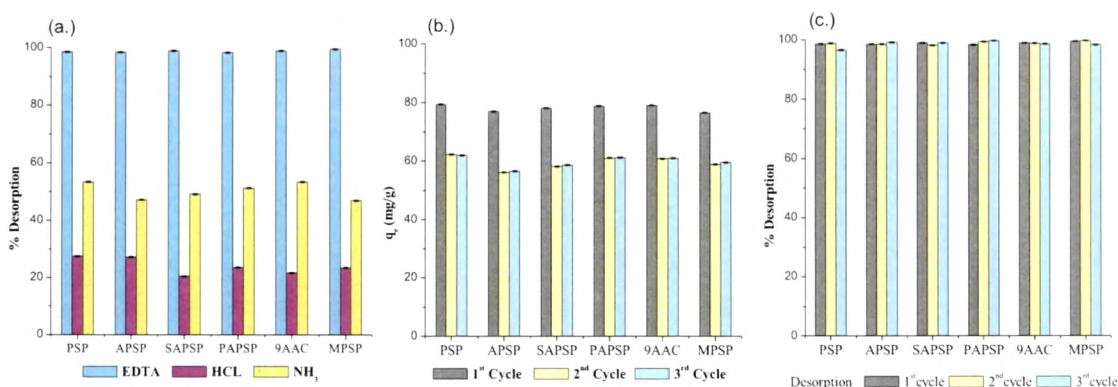


**Figure 5.9.** Column Modeling studies



### 5.3.8. Desorption.

Solutions of 0.1 M HCl, 0.1 M EDTA and 0.1 M  $\text{NH}_3$  have been studied as eluents for desorption of  $\text{U}^{6+}$ . From Figure 5.10 it is evident that desorption of  $\text{U}^{6+}$  from the metal-loaded adsorbents with 0.1M EDTA resulted in >99% recovery.



Operating parameters: Adsorption: 30  $^{\circ}\text{C}$ , 180 min, pH 1, 1000 ppm, 0.1 g adsorbent, 180 rpm. Desorption: 0.1 N desorbent, desorbing time: 30 min, 30  $^{\circ}\text{C}$ .

**Figure 5.10.** Desorption and cycles of adsorption (a) Effect of desorbents (b) Cycles of adsorption (c) Cycles of desorption

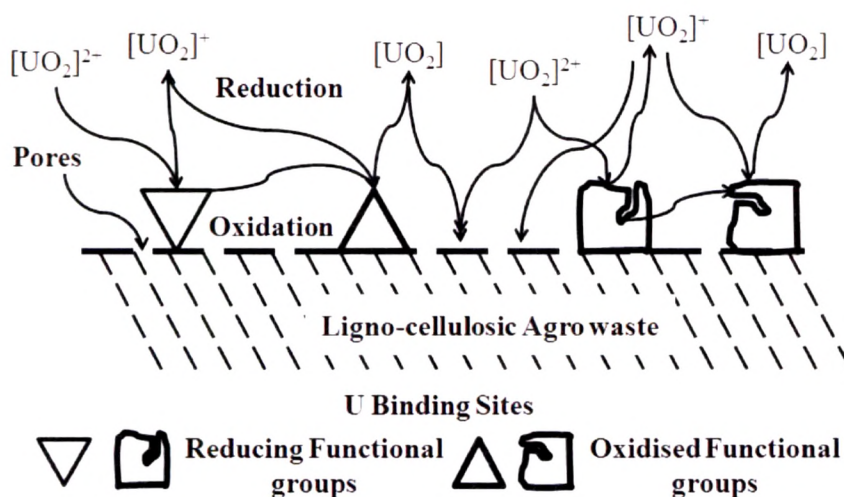
This indicates that ion exchange is involved in the adsorption process [55]. However, the use of 0.1M  $\text{NH}_3$  and 0.1 M HCl resulted in >48 and >20 % recovery of  $\text{U}^{6+}$  respectively. It was observed that  $\text{U}^{6+}$  was easily desorbed within 30 min, which would prove highly advantageous for metal recovery. From Figure 5.10 it is evident that the removal capacity of adsorbents shows insignificant changes in the second and third cycle. Thus regeneration and reuse of the adsorbents under study is an economical and efficient method for removal of  $\text{U}^{6+}$  from water.

### 5.4. Mechanism.

The possible mechanisms for the removal of uranium include: complexation or chelation of uranyl or reduced uranous species by organic ligands, adsorption by weak van der Waals and hydrogen bonding. Although sorption onto the adsorbents under study is likely to be responsible for the initial removal of U from solution, some subsequent surface reduction of U(VI) to U(IV) occurs. The reduction of uranium occurred concurrently with the oxidation of hydroxyl and aldehydic groups. Interestingly, U(V) which is not supposed to be stable is seen to be stabilized

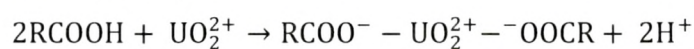
by the reducing groups present in the adsorbents under study. Reduction of uranyl species by the reducing groups under right pH conditions to relatively insoluble  $\text{UO}_2$  and  $\text{U(V)}$  and precipitation could be taking place.

The reduction of  $[\text{UO}_2]^{2+}$  to  $\text{U(IV)}$  is thought to proceed *via* single electron transfer to pentavalent uranyl,  $[\text{UO}_2]^+$  and further reduction to  $[\text{UO}_2]$  as shown in scheme 5.1.

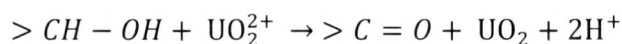


**Scheme 5.1.** Redox mechanism for uranium adsorbed species

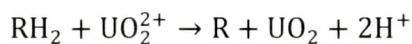
The interaction of uranyl ions with the adsorbents under study can take place as below. Formation of uranyl carbonyl complexes:



Oxidation of hydroxyl groups in the adsorbents into carbonyl groups:



Dehydrogenation of aliphatic hydro-carbonaceous moieties are known to be 'catalyzed' by uranium species [56].



## 5.5. Conclusions

The adsorption potential of PSP, APSP, SAPSP, PASP, 9AAC and MPSP towards adsorption of uranium was evaluated. The parameters influencing the adsorption process like pH, dose of adsorbent and agitation time were optimized. Sorption isotherms of U(VI) on the adsorbents under study were evaluated using Freundlich, Langmuir, Temkin, Dubinin-Radushkevich (DR), Flory-Huggins, Elovich and Halsey isotherms. The values of  $E_0$  derived from DR model suggest ion exchange as the working mechanism for APSP, SAPSP, MPSP and PAPS, particle diffusion for PSP while for 9AAC the value suggests physisorption. The  $\Delta G^0$  values from Langmuir and thermodynamic calculations indicate physisorption as the major mechanism for adsorption of uranium. The adherence to pseudo second order kinetic model and Halsey model indicate multilayer and ion exchange as the mode of adsorption thus justifying our hypothesis that a range of mechanisms are involved in the adsorption process to different extents for the adsorbents under study. We have observed for the first time that the adsorption of uranium takes place by adsorption followed by reduction, the reduced species being both U(IV) and U(V). The sorption process was found to be exothermic, spontaneous and accompanied by decrease in entropy. Furthermore data also suggest that the adsorbents under study prepared from biomass, particularly APSP and PAPS may be an inexpensive and viable means to remediate  $\text{UO}_2^{2+}$  from contaminated acidic solutions as till date adsorbents with good adsorption capacity at low pH (~1) are not available in literature.

## Literature Cited.

1. A. Nakajima, T. Tsuruta. *J. Nucl. Sci. Technol.* **2002**, 528.
2. K.C. Bhainsa, S.F. D'Souza. *J. Environ. Sci. Health, Pt. A: Toxic/Hazard. Subst. Environ. Eng.* **2001**, A36, 1621.
3. M.T. Gonzalez-Munoz, M.L. Merroun, N.B. Omar, J.M. Arias. *Int. Biodeterior. Biodegrad.* **1997**, 40, 107.
4. J. Yang, B. Volesky. *Environ. Sci. Technol.* **1999**, 33, 4079.
5. K. Popa, A. Cecal. *Environ. Eng. Manage. J.* **2003**, 2, 69.
6. M. Jansson-Charrier, E. Guibal, J. Roussy, R. Surjous, P. Le Cloirec. *Water Sci. Technol.* **1996**, 34, 169.
7. T.S. Psareva, O.I. Zakutevskyy, N.I. Chubar, V.V. Strelko, T.O. Shaposhnikova, J.R. Carvalho, M.J.N. Correia. *Colloids Surf. A* **2005**, 252, 231.
8. W.J. Liu, W.C. Xu, B.E. Wang. *Youkuangye* **2004**, 23, 143.
9. T.A. Davies, B. Volesky, A. Mucci. *Water Res.* **2003**, 37, 4311.
10. M. Kalin, W.N. Wheeler, G. Meinrath. *J. Environ. Radioactiv.* **2005**, 78, 151.
11. J. Wang, C. Chen. *Biotechnol. Adv.* **2006**, 24, 427.
12. K.J. Tiemann, G. Gamez, K. Dokken, J.G. Parsons, J.L. Gardea-Torresdey. *Microchem. J.* **2002**, 71, 287.
13. A.A. Atia, *Hydrometallurgy* **2005**, 80, 13.
14. E.D. Vecchia, H. Veeramani, E.I. Suvorova, N.S. Wigginton, J.R. Bargar, R.B. Latmani. *Research in Microbiology* **2010**, 161, 765.
15. L. Alidokht, A.R. Khataee, A. Reyhanitabar, S. Oustan. *Desalination* **2011**, 270, 105.
16. S.B. Savvin, *Talanta* **1961**, 8, 673.
17. M.M. Abou-Mesalam, I.M. El-Naggar, M.S. Abdel-Hai, M.S. El-Shahawi, *J. Radioanal. Nucl. Chem.* **2003**, 258, 619.
18. M.S. El-Shahawi, M.A. Othman, M.A. Abdel-Fadeel, *Anal. Chim. Acta* **2005**, 546, 221.
19. M.S. El-Shahawi, M.A. Othman, H.M. Nassef, M.A. Abdel-Fadeel, *Anal. Chim. Acta* **2005**, 536, 227.
20. E.M. Saad, R.A. Mansour, A. El-Asmy, M.S. El-Shahawi. *Talanta* **2008**, 76, 1041.
21. G. Meinrath. *Journal of Radioanalytical and Nuclear Chemistry* **1998b**, 232, 179.

22. W. Dong, S.C. Brooks. *Environ. Sci. Technol.* **2006**, 40, 4689.
23. S.K. Das, A.R. Das, A.K. Guha. *Environ. Sci. Technol.* **2007**, 41, 8281.
24. K.V. Kumar, K. Porkodi. *J. Hazard. Mater.* **2007**, 146, 214.
25. J. Febrianto, A.N. Kosasih, J. Sunarso, Y.H. Ju, N. Indraswati, S. Ismadji. *J. Hazard. Mater.* **2009**, 162, 616.
26. R.S. Vieira, M.M. Beppu. *Colloids Surf. A.* **2006**, 279, 196.
27. Y.S. Ho, G. McKay. *Chem. Eng. J.* **1998**, 70, 115.
28. S. Schiewer, S.B. Patil. *Biores. Technol.* **2008**, 99, 1896.
29. Z. Reddad, C. Gerente, Y. Andres, P.L. Cloirec. *Environ. Sci. Technol.* **2002**, 36, 2067.
30. K. Vijayaraghavan, K. Palanivelu, M. Velan. *Biores. Technol.* **2006**, 97, 1411.
31. J. Sarma, A. Sarma, K.G. Bhattacharyya. *Ind. Engg. Chem. Res.* **2008**, 47, 5433.
32. C. Gerente, V.K.C. Lee, P.L. Cloirec, G. McKay. *Crit. Rev. Environ. Sci. Technol.* **2007**, 37, 41.
33. V.K. Gupta, I. Ali, V.K. Saini, T.V. Gerven, B.V. Bruggen, C. Vandecasteele. *Ind. Eng. Chem. Res.* **2005**, 44, 3655.
34. G.J.L. Torresdey, K. Dokken, K.J. Tiemann, J.G. Parsons, J. Ramos, N.E. Pingitore, G. Gamez,. *Microchem. J.* **2002**, 71, 157.
35. M.M. Figueira, B. Volesky, H.J. Mathieu. *Environ. Sci. Technol.* **1999**, 33, 1840.
36. E. Fourest, B. Volesky. *Environ. Sci. Technol.* **1996**, 30, 277.
37. N.B. Clothup, L.H. Daly, S.E. Wiberley, Introduction to Infrared and Raman Spectroscopy, 3<sup>rd</sup> ed.; Academic Press: London, **1990**.
38. Z.Y. Lin, J.M. Wu, B.Q. Fu, R. Xue, J.Z. Zhou, Q.X. Zheng, Y.Y. Liu, J.K. Fu. *Acta Chim. Sinica* **2004**, 62, 1829.
39. W.J. Liu, W.C. Xu, B.E. Wang. *Environ. Prot. Sci.* **2004**, 30, 39.
40. M.A. Rashid. *Chem. Geol.* **1972**, 9, 241.
41. P. Ioselis, R. Ikan, M. Frenkel. Thermal degradation of metal complexed humic substances. In: A.G. Douglas and J.R. Maxwell (Eds), *Advances in Organic Geochemistry*, Pergamon Press, **1979**, 547.
42. Y.K. Kharaka, W.W. Carothers, R.J. Rosenbauer. *Geochim. Cosmochim. Acta* **1983**, 47, 397.
43. S. Fonglim, Y. Mingzheng, S. Wenzou, J.P. Chen. *Environ. Sci. Technol.* **2008**, 42, 2551.
44. R.L. Frost. *Spectroc. Acta. A. Mol. Biomol. Spectrosc.* **2006**, 64, 308.
45. M. Tsezos, B. Volesky. *Biotechnol. Bioeng.* **1982**, 24, 385.



46. C.A. Tellez Soto, M. Arissawa, J. Gomez Lara, M.A. Mondragon. *Polyhedron* **2000**, 19, 2353.
47. P.L. Arnold, J.B. Love, D. Patel. *Coordination Chemistry Reviews* **2009**, 253, 1973.
48. F.A. Cotton, G. Wilkinson, *Advanced Inorg. Chem.* Willey Eastern Pvt, **1969**.
49. S. Bera, S.K. Sali, S. Sampath, S.V. Narasimhan, V. Venugopal. *Journal of Nuclear Materials* **1998**, 255, 26.
50. J.H. Liu, S. Vanden Berghe, M.J. Konstantinovic. *Journal of Solid State Chemistry* **2009**, 182, 1105.
51. J.J. Pireaux, J. Riga, E. Thibaut, C. Tenret-Neol, R. Caudano, J.J. Verbist, *Chem. Phys.* **1977**, 22, 113.
52. G.C. Allen, P.M. Tucker, J.W. Tyler, *J. Phys. Chem.* **1982**, 86, 224.
53. X. Tan, Q. Fan, X.B. Wang. *Environ. Sci. Technol.* **2009**, 43, 3115.
54. S.S. Baral, N. Das, T.S. Ramulu, S.K. Sahoo, S.N. Das, G.R. Chaudhury. *J. Hazard. Mater.* **2009**, 161, 1427.
55. L. Xiaomin, Y. Tang, C. Xiuju, L. Dandan, L. Fang, W. Shao. *Colloids and Surfaces A: Physicochem. Eng. Aspects* **2008**, 317, 512.
56. S. Choudhary, P. Sar. *Journal of Hazardous Materials* **2011**, 186, 336.